Hindawi
International Journal of Energy Research
Volume 2023, Article ID 6846467, 15 pages
https://doi.org/10.1155/2023/6846467

WILEY | Hindawi

Research Article

A Design and Optimization Methodology for Liquid Metal Fast Reactors

Khaldoon Al-Dawood and Scott Palmtag

North Carolina State University, USA

Correspondence should be addressed to Scott Palmtag; sppalmta@ncsu.edu

Received 18 October 2022; Revised 30 January 2023; Accepted 24 February 2023; Published 8 March 2023

Academic Editor: Andrey Kuzmin

A liquid metal fast reactor (LMFR) design and optimization methodology (DOM) has been developed. The methodology effectively explores a search space by initially sampling the search space, excluding invalid design samples prior to performing expensive multiphysics analysis, and then performing local searches of the design space. The design samples are evaluated using the multiphysics capabilities of the LUPINE LMFR simulation suite. Two studies have been performed to demonstrate DOM. First, the Westinghouse long-life core lead fast reactor (WLFR) is optimized. This reactor is 950 MW_{th} and fueled with uranium nitride (UN) fuel which has a natural nitrogen isotopic abundance. The objective of the optimization is the reduction of the levelized fuel cycle cost (LFCC) while complying with the design constraints. Considering the challenges associated with using natural nitrogen in nitride fuel, a second study was performed to design a competitive ^{15}N-enriched UN-fueled long-life core LFR. Based on this design, the cost of the ^{15}N enrichment process necessary to achieve a competitive LFCC was calculated.

1. Introduction

The current fleet of commercial nuclear power plants in the United States is based solely on light water reactor (LWR) technology. Advanced reactors are being developed that can offer improved safety, economics, nuclear fuel utilization, and proliferation resistance to meet future energy needs. The Generation IV International Forum (GIF) evaluated 130 advanced reactor concepts and identified six promising technologies for the next generation of nuclear power. Two of the six technologies were liquid metal fast reactors (LMFRs). These technologies were the sodium fast reactor (SFR) and the lead fast reactor (LFR). Several LFRs are under development worldwide, including the Westinghouse lead-cooled fast reactor in the United States [1], the advanced lead fast reactor European demonstrator (ALFRED) in Europe [2], BREST-OD-300 in Russia, and the proliferation-resistant environmental-friendly accident-tolerant continuable and economical reactor (PEACER) in the Republic of Korea [3]. This work has been developed to aid in the efficient design of LFRs.

The design and optimization of reactor cores are key for improving the economy of the fuel cycle and the safety of the core. At a basic level, the design of LMFR cores considers neutronics, thermal hydraulics, structural mechanics, and economics phenomena. A reactor core design process can be summarized in three steps. In the first step, the objectives, constraints, and materials to be used in the technology are identified. In the second step, the preliminary reactor design is conceptualized. In the third step, the reactor design is optimized.

Traditionally, the preliminary design step is done by an experienced designer. The process requires starting with a good initial guess. The designer then iterates over the design trying to improve the economic, thermal hydraulics, structural mechanic, and safety performances of the core. After this, depending on the design objectives and nature of the design process, the designer can decide the strategy, algorithm, and tools to explore an optimized reactor core design.

LWR design is relatively mature and the geometry rarely changes. Therefore, in LWRs, the predominant style of optimization in core design is a combinatorial optimization

which is concerned with finding an optimal fuel arrangement. Examples of such a problem include boiling water reactor (BWR) fuel assembly design and pressurized water reactor (PWR) fuel core loading design. Such problems feature a large search space that can grow up to 10^{31} possible evaluations. Several approaches for optimizing this problem are found in the literature. Examples include, but are not limited to, simulated annealing [4, 5], reinforced learning [6], Tabu search [7], particle swarm algorithm [8], and genetic algorithms [9].

Compared to LWRs, LMFR geometry is still unknown, and a feasible geometry must be searched in the design process. The thermal hydraulic-neutronic coupling is weak in LMFRs. This is due to two factors. First, the liquid metal in an LMFR is only a coolant (i.e., no moderation as in LWRs). Second, the axial variation in the liquid metal coolant density in LMFR is small compared to that of water coolant in LWRs. As a result of this weak coupling, the process of attaining a reliable design is more flexible. Thus, in the preliminary design process for LMFRs, the focus is expected to be on finding a reliable geometry for the fuel assembly. In addition, fast reactors have a much larger neutron mean-free-path and are more tightly coupled than an LWR. Therefore, it is important to perform the optimization on a full-core level. In literature, methodologies for the preliminary design of LMFR cores take the style of an iterative process to attain a fuel assembly design. As an example, the assembly design and optimization (ADOPT) was developed to perform LMFR assembly design [10]. ADOPT performs an iterative multiphysics (geometric, neutronic, structural mechanic, and thermal hydraulic) evaluation of the assembly design. ADOPT uses objectives and constraints provided by the user to derive an initial guess. Then, by iterating over the different code modules, an optimized core geometry is achieved. The methodology in ADOPT focuses on the design and optimization of reactor cores with the breed and burn operation strategy.

Another methodology for the design and optimization of the LMFR core was suggested and implemented in the core design and optimization (CODOPT) code [11]. CODOPT iterates between three modules. These are the geometry, neutronics, and thermal hydraulics modules. The coupling between the neutronics and thermal hydraulics considers the variation of material temperature. The code was used to optimize the M^2LFR-1000 LFR core [12].

In this work, a new general-purpose exploratory design and optimization methodology (DOM) for LMFRs is proposed. The methodology follows the constrained nuclear design principles [13] and uses a noniterative approach. DOM is based on two principles. These are the efficient sampling of the search space and performing initial screening on the samples to identify invalid ones prior to performing the expensive multiphysics calculations. In the current implementation of DOM, the core analysis is performed using the multiphysics simulation suite LUPINE [14]. The physics accounted for in the analysis are neutronics, thermal hydraulics, thermal expansion, and fuel cycle cost as summarized in Figure 1. DOM is suggested to replace the preliminary design in the traditional design process and dispenses with the iterative process between different physics. The future development of DOM can be improved by introducing more physics to the analysis, including fuel performance and safety analysis.

DOM was demonstrated through two scenarios. Both scenarios were searched to achieve a reliable reactor geometry and fuel enrichment. In the first scenario, the Westinghouse long-life core LFR (WLFR) was optimized with the objective of reducing the levelized fuel cycle cost (LFCC). In the second scenario, ^{15}N-enriched uranium nitride-(UN-) fueled long-life core LFR is designed. The rationale behind the second scenario is the realization of the advantages of utilizing ^{15}N in the fuel instead of ^{14}N, as will be described in Section 6. Based on this new design, the cost of ^{15}N enrichment process required to make the fuel cycle economically competitive is calculated.

The paper is organized as follows. A general description of DOM is presented in Section 2. The WLFR design is presented in Section 3. The theory and details of applying DOM to LMFRs design and optimization is presented in Section 4. In Section 5, the results of the first demonstration scenario are presented. Section 6 studies the buildup of ^{14}C in the original WLFR and the new design found by DOM for the ^{15}N-enriched UN-fueled LFR core. The conclusions of this work are presented in Section 7.

2. The Design and Optimization Methodology (DOM)

Optimization is the process of finding system inputs which result in the best outcome(s) of that system. The traditional and obvious method of investigating a search space is to use a full factorial design. To do a full factorial design, the search space is first discretized, and the objective function is evaluated for every possible combination of explanatory variables on the grid. Depending on the number of explanatory variables and the size of the discretization, the number of possible cases can grow large, rendering the problem computationally expensive. Instead of evaluating every combination of explanatory variables in the space, the computational burden can be alleviated by performing the sampling. Sampling methods include Monte Carlo (MC) sampling or design of experiment (DOE) sampling (Latin hypercube sampling (LHS) is a well-known example of DOE).

DOM is suggested as a methodology for the efficient exploration of a search space. The methodology achieves its goal by applying two principles. The first is the efficient sampling of the search space. The second is the initial identification of invalid design samples withdrawn from the search space prior to performing computationally demanding multiphysics analysis. In applying the second principle, a simplified initial screening method is set up. Design samples are evaluated using the screening method and rejected if they violate the design constraints. Design samples that pass the initial screening are evaluated using the multiphysics analysis. After this, the results from the multiphysics analysis are compared again against the design constraints. Cases that violate the constraints are excluded from further processing. For the rest of the cases, the objective function

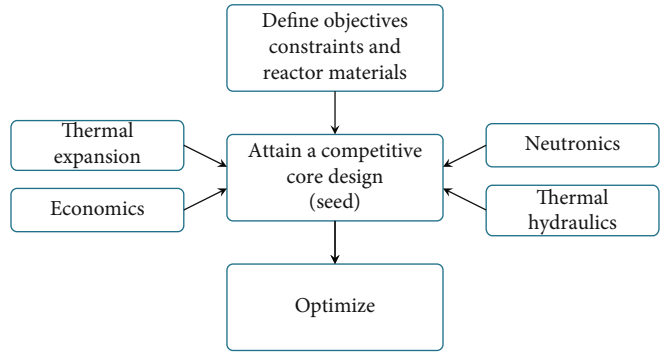

Figure 1: General design process using DOM.

is calculated, and seeds are identified. A seed is a design sample that is believed to be close to local or global optima. After this, a local optimization can be used to find an optimized design. The application of DOM for the design of LMFRs as used in this work is presented in Section 4.

3. Westinghouse Long-Life Core LFR (WLFR)

Recently, the long-life LMFR design has been recognized as an economical option for LMFRs operation. A long-life core can be broadly defined as a 20+ year core that does not shuffle or refuel the reactor core. The long-life core has some practical and economic advantages. For example, a long refueling interval does not have reactor refueling outages, which increases the operational capacity factor. In addition, with the absence of fuel shuffling, refueling equipment is not required on the reactor site. From a proliferation point of view, the reactor vessel is sealed for a very long time, which results in reduced proliferation risk. On top of this, with the long-life operation strategy, such reactors can be used in remote places where other sources of energy can be expensive and/or impractical. Due to these advantages, LMFR long-life core concept has been suggested with different sizes and for different purposes [15–17]. Some long-life core concepts are more mature and have been studied extensively. Examples include the constant axial shape of neutron flux, nuclide densities, and power shape during life of energy production (CANDLE) SFR [18] and the small secure transportable autonomous reactor (SSTAR) LFR [19]. As mentioned earlier, the WLFR [1] was used to demonstrate DOM in this work. The WLFR will serve as the reference core for the DOM optimization. In this section, the WLFR design description and constraints are presented.

The WLFR is a 950 MW_{th}, modular, medium size, lead-cooled fast spectrum reactor. The design leverages the benefits of long refueling intervals to achieve economic competitiveness. The reactor core uses UN fuel with natural nitrogen composition. The selection of UN fuel is based on its superior neutronic and thermomechanical behavior, in addition to its compatibility with reactor materials and liquid metal coolants.

The reactor uses hexagonal fuel assemblies. Due to pressure drop and coolant speed constraints, the WLFR fuel assemblies were designed with large pins and large pin spacing. Due to the corrosive and erosive nature of liquid lead to structural material, a soft constraint of 2 m/s was imposed on the lead speed in the WLFR. It should be noted that the maximum allowed lead coolant speed in the literature ranges between 2 m/s and 3 m/s [20]. Due to the large spacing between the fuel pins, a spacer grid is used to support the fuel pins, compared to the more tightly packed SFR fuel assembly designs that use wire wraps for fuel pin spacing. The clad and structural materials for the reactor are made of the double-stabilized low-swelling austenitic steel (DS4). The loose fuel lattice packing does not negatively impact the neutronic performance of the core because of the large atomic mass nuclei of lead, which constricts their ability to moderate fast neutrons. The initial reactor design was optimized using the coupling of the DAKOTA code with the Argonne National Laboratory (ANL) fast reactor code suite [1]. The specifications of the WLFR are shown in Table 1. The design objectives and constraints are presented in Table 2. The initial fuel assembly design is presented in Table 3.

A midplane view of the core is shown in Figure 2. The core is composed of three radial regions with different levels of ^{235}U enrichment. These regions are referred to as the inner core, middle core, and outer core which are denoted as IC, MC, and OC, respectively, in Figure 2. The fuel assemblies have a constant axial composition in the fuel region. The active core is radially surrounded by a ring of reflector assemblies (denoted as REF) and a ring of shield assemblies (denoted as RSH). Reactor control is achieved by control rods and safety rods. The location of the control and safety rods in the core map is denoted as EMP. The core has a sixth-core symmetry, which is used in the simulation to reduce the computational cost. It should be mentioned that no control rod models were considered in the studies presented in this work. The control and safety rod locations were modeled as ducts filled with coolant.

The modeling and simulation of LFRs in this work were performed using the multiphysics suite LUPINE [14]. More details will be provided on LUPINE in Section 4.3. The core was depleted for 25 effective full power years (EFPY). This cycle length was selected to match the cycle length of the original WLFR design [1]. Figure 3 shows a beginning-of-cycle (BOC) and end-of-cycle (EOC) power distribution in the WLFR sixth-core model active fuel region. The figure shows that the WLFR power peaking shifts from the periphery of the core towards the center as the core depletes.

Table 1: WLFR general reactor specifications [1].

Parameter	Value
Core power (MW_{th})	950
Structural and cladding material	DS4
Total number of assembly locations	451
Number of fuel assemblies	289
Active fuel height (cm)	220.0
Coolant inlet temperature (K)	693.15
Number of core enrichment regions	3
Cycle length (EFPY)	25
Average coolant velocity (m/s)	1.49
Inner core enrichment (%)	10.3
Middle core enrichment (%)	11.8
Outer core enrichment (%)	13.8
Fuel porosity (%)	15

Table 2: Constraints of the WLFR [1].

Parameter	Value
Maximum clad surface temperature (K)	1023
Maximum fuel temperature (K)	1773
Maximum fuel burnup (MWd/kgHM)	200
Fuel enrichment (%)	<19.9
Coolant speed (m/s) (soft constraint)	<2
Target refueling interval (years)	10-30
Interassembly gap (cm)	0.4

4. Application of DOM in LMFR Design

For the specific application of DOM in the design of long-life core LMFRs, the process can be summarized in six steps, which are presented in Figure 4. A Python program was written to perform the steps in the DOM design process. This section contains a detailed description of each step in this process.

4.1. Sampling the Search Space. The most popular DOE approach is the LHS. Compared to MC, LHS is known for a better coverage of the search space for a certain budget of samples [21]. LHS is a space-filling DOE approach aiming to generate evenly-spread design samples across a search space [22]. In the simplest form of performing LHS, assume that one is interested in sampling p points from a d-dimensional space. The matrix $\mathbf{X} = [\mathbf{x_1}, \mathbf{x_2}, \cdots \mathbf{x_p}]^{\mathbf{T}}$ contains the total samples. Row $\mathbf{x}_i = [x_i^{(1)}, x_i^{(2)} \cdots x_i^{(d)}]$ represents the i^{th} sample. The LHS algorithm divides each dimension of the d-dimensional space into p strata with marginal probability of $1/p$ on a square grid and samples the design parameters such that there is only one sample in each variables bin (i.e., called Latin hypercube) [23].

As a simple demonstration for the LHS, a two-dimensional search space can be used. Figure 5 shows five samples withdrawn from a bivariate search space using LHS. In this figure, one can notice that the space was sampled with one (and only one) sample in each variable bin. LHS was used in this work to sample the search space.

Table 3: WLFR assembly design [1].

Parameter	Value
Assembly pitch (cm)	16.3
Pitch-to-diameter ratio	1.143
Number of fuel pins per assembly	61
Fuel pellet radius (cm)	0.7524
Fuel pin radius (cm)	0.8485
Fuel pin pitch (cm)	1.8925
Active fuel height (cm)	220
Inner core enrichment (%)	10.3
Middle core enrichment (%)	11.8
Outer core enrichment (%)	13.8

For the application of DOM in LMFR design, the parameters that constitute the search space were the pin radius (R), pin pitch-to-diameter (P/D) ratio, fuel height (H), fuel assembly pitch (P_A), and three core zone enrichments. It should be noted that the P/D ratio sampling in DOM is used to select the number of fuel pins per assembly.

The LHSs are generated in this work using the Latin hypercube sampling with multidimensional uniformity (LHSMDU) package in Python [24, 25]. The LHSMDU-generated samples are normalized on $\zeta_i \in [0, 1]$. Assuming that an explanatory variable X is to be sampled in the domain $[X_{\min}, X_{\max}]$, the sample X_i can be calculated according to

$$X_i = X_{\min} + \zeta_i (X_{\max} - X_{\min}). \tag{1}$$

Once the samples are prepared, the geometric explanatory variables of a sample will be used to derive other geometric parameters in the assembly design. The number of fuel pins per assembly is obtained using the design sample assembly pitch, fuel pin radius, and the P/D ratio. It is calculated by populating fuel channel rings in the fuel assembly in an iterative process and comparing the diagonal inside the assembly duct to the span of the fuel channels across the diagonal. A demonstration of this process is provided in Figure 6. The clad thickness is calculated using the pin radius using a user-provided cladding thickness ratio (CTR) [10] which is defined as

$$\text{CTR} = \frac{t_{\text{clad}}}{\text{2R}}. \tag{2}$$

The CTR utilized in this work is 0.05358 as calculated from the original design [1]. Similar to the CTR concept, the assembly duct thickness was calculated using a user-provided duct thickness ratio (DTR) which is defined as

$$\text{DTR} = \frac{t_{\text{duct}}}{\text{P}_\text{A}}. \tag{3}$$

While a more accurate method for calculating the clad and duct thicknesses in an LMFR can be used, the DTR

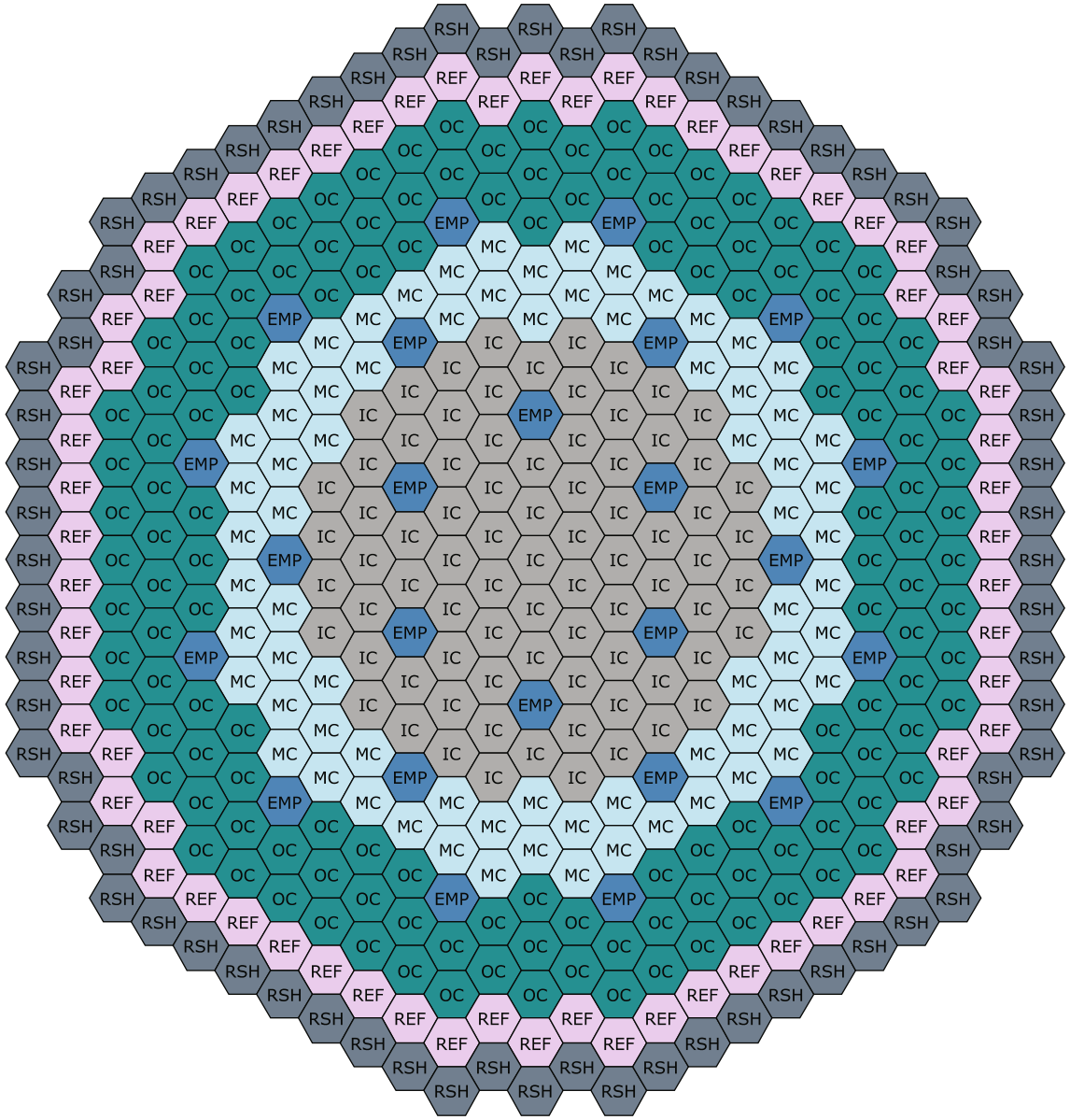

Figure 2: Midplane view of the WEC long-life core LFR.

and CTR concepts are provided as a means to calculate reasonable values for these design parameters. Finally, the fuel-cladding gap thickness and interassembly gap were selected to be 5.13×10^{-3} cm and 0.4 cm, respectively, for all design samples.

4.2. Initial Thermal-Hydraulic Screening. In the second step of DOM (as in Figure 4), the method attempts to identify invalid design samples withdrawn from the search space and exclude them before being evaluated with the computationally expensive multiphysics analysis tools. A simplified thermal-hydraulic model was built and used to perform this initial screening step. The following is a description of the screening process.

Based on assumptions of the radial (r_p) and axial (r_z) power peaking factors, a hottest fuel channel model is constructed for each design sample produced in the sampling process. The hottest channel model consists of one-dimensional steady-state axial convection and radial conduction solutions from which the fuel pin component temperatures are calculated. If the model shows a violation for the design constraints, the sample will be excluded from further processing. The user can control the number of rejected designs by adjusting the peaking factors assumed. With this, the user can control the degree of conservatism in the exploration process.

The power peaking factor is related to the linear power density as

$$r = r_p \times r_z = \frac{q'_\circ}{q'_{\text{avg}}}, \tag{4}$$

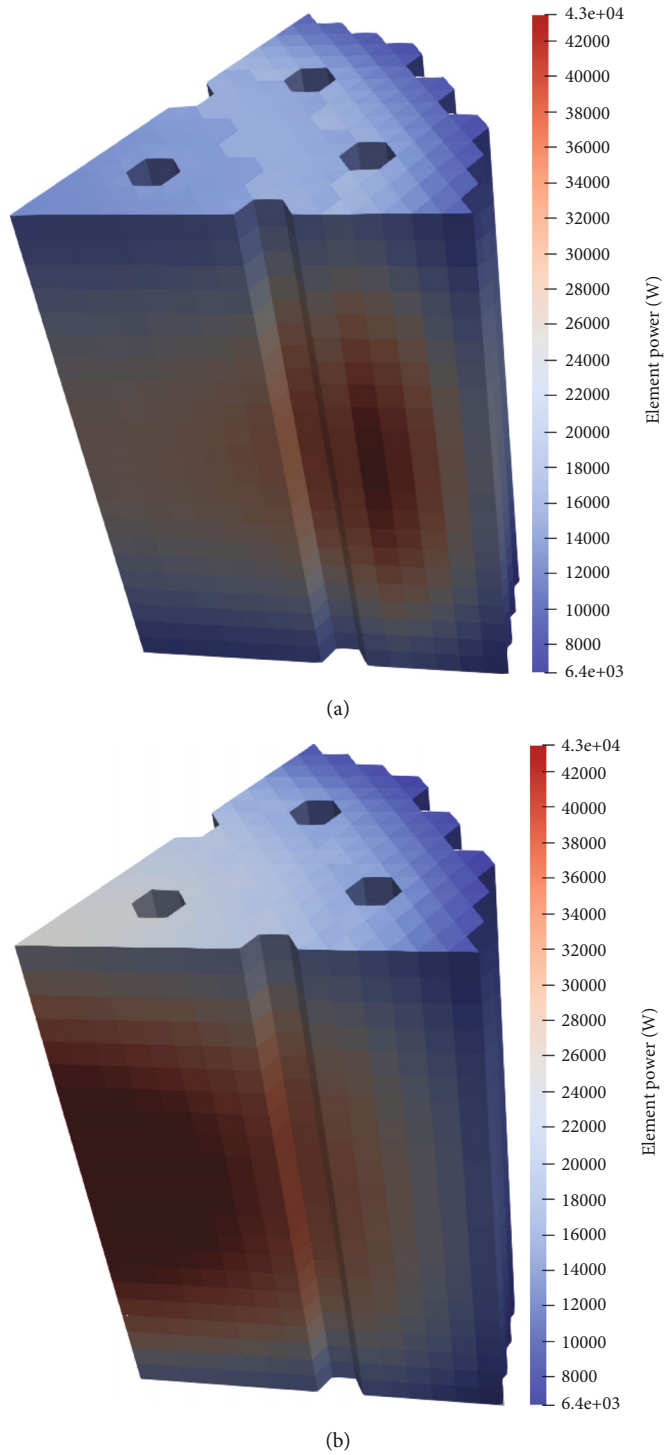

Figure 3: (a) BOC and (b) EOC power distribution of WEC long-life core LFR active core region.

where $q'_{\circ}$ and q'_{avg} are the maximum and average linear power densities in the core, respectively.

The axial linear power profile for the hottest channel model is assumed to have a chopped-cosine function shape.

$$q'(z) = q'_o \cos\left(\frac{\pi z}{L\chi}\right), \tag{5}$$

where L is the active fuel height and $z \in [-L/2, L/2]$ is the axial location in the fuel element. χ is the chopped-cosine factor. To calculate χ, the average linear power density for the hottest channel is calculated using Equation (5).

$$q'_{\text{avg},\circ} = \frac{1}{L}\int_{-L/2}^{L/2} q'(z)\mathrm{d}z = q'_{\text{avg}} \times r_p. \tag{6}$$

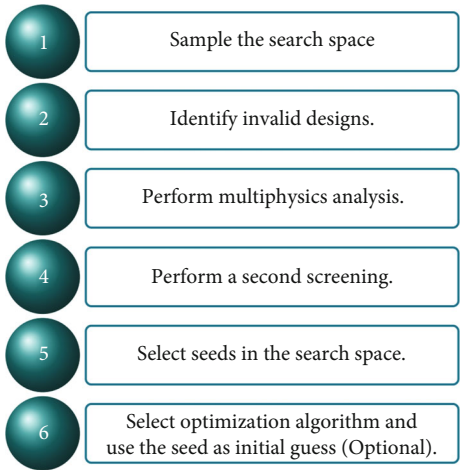

Figure 4: Steps of using DOM in the process of designing LMFRs.

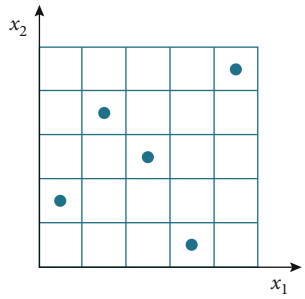

Figure 5: Example of withdrawing 5 samples from a bivariate search space using LHS.

As a result, the converted axial peaking factor can be calculated by solving Equation (7) for χ

$$r_z = \frac{\pi}{2\chi \sin(\pi/2\chi)}. \tag{7}$$

The hottest fuel pin is axially divided into K axial zones as shown in Figure 7. In each axial zone, an energy balance equation is solved to obtain the zone exit temperature. The energy balance in an axial zone j is presented in the following equation:

$$\dot{m}\int_{T_{j,\text{in}}}^{T_j(z')} C_p(T)dT = \int_{z_{j,\text{in}}}^{z'} q'_o \cos\left(\frac{\pi z}{\chi L}\right)dz, \tag{8}$$

where $z' \in [z_{j,\text{in}}, z_{j,\text{out}}]$. The axial levels $z_{j,\text{in}}$ and $z_{j,\text{out}}$ are the axial elevation of the inlet and outlet of the axial zone j, respectively. $C_p(T)$ is the heat capacity of the coolant at temperature T. Given that the core coolant inlet temperature is known, the energy balance can be used to solve for the coolant temperature along the whole hottest channel model. If the axial zone height is small enough, Equation (8) can be reduced to

$$\dot{m}C_p\left(T_{j,\text{in}}\right)\int_{T_{j,\text{in}}}^{T_j(z')} dT = \int_{z_{j,\text{in}}}^{z'} q'_o \cos\left(\frac{\pi z}{\chi L}\right)dz. \tag{9}$$

By solving Equation (9) for $T_j(z')$, the coolant temperature as a function of elevation in zone j can be calculated according to Equation (10). When $z' = z_{j,\text{out}}$, Equation (10) calculates the outlet temperature of zone j.

$$T_j(z') = T_{j,\text{in}} + \frac{q'_o \chi L}{\pi \dot{m} C_p\left(T_{j,\text{in}}\right)} \times \left(\sin\left(\frac{\pi z'}{\chi L}\right) - \sin\left(\frac{\pi z_{j,\text{in}}}{\chi L}\right)\right). \tag{10}$$

At each axial zone, the zone coolant outlet temperature is used to calculate the material temperatures radially in the fuel pin using the steady-state convection and conduction models. Using Newton's cooling law, the outer clad surface temperature in zone j can be calculated as follows:

$$T_{j,\text{oc}} = T_{j,\text{out}} + \frac{q'_j}{2\pi h_j r_{\text{oc}}}, \tag{11}$$

where h_j is the heat transfer coefficient. It is calculated using

$$h_j = \frac{\text{Nu}_j \times k\left(T_{j,\text{out}}\right)}{D_e}, \tag{12}$$

where $k(T)$ is the coolant conductivity and Nu is the Nusselt number, which can be calculated using the Subbotin-Ushakov correlation [26, 27].

$$Nu_j = 7.55\frac{P}{D} - 20\left(\frac{P}{D}\right)^{-13} + \frac{3.67}{90(P/D)^2} \times Pe^{0.56+0.19\times P/D}, \tag{13}$$

where the P/D is the pin pitch-to-diameter ratio. It should be noted that the correlation is valid on $1.0 \le P/D \le 2.0$ [27]. This correlation for the Nusselt number can be used for both sodium and lead coolants.

A one-dimensional conduction equation is solved in the cladding to obtain the temperature in the inner cladding surface. The cladding inner surface temperature can be calculated using the cladding outer surface temperature as

$$T_{j,\text{ci}} = T_{j,\text{co}} + \frac{q'_j}{2\pi k_c} \ln\left(\frac{r_{\text{oc}}}{r_{\text{ci}}}\right), \tag{14}$$

where k_c is the clad conductivity, r_{ci} is cladding inner radius and r_{co} is the clad outer surface radius. Another one-dimensional conduction model is developed for the gap

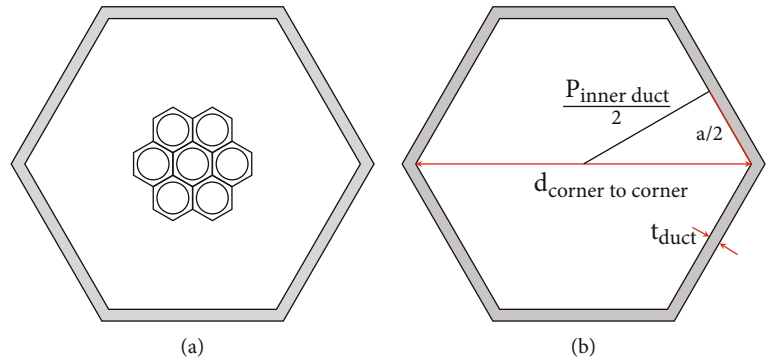

Figure 6: Process of calculating the number of pins in a fuel assembly (a) populating rings (b) compare to inner duct diagonal.

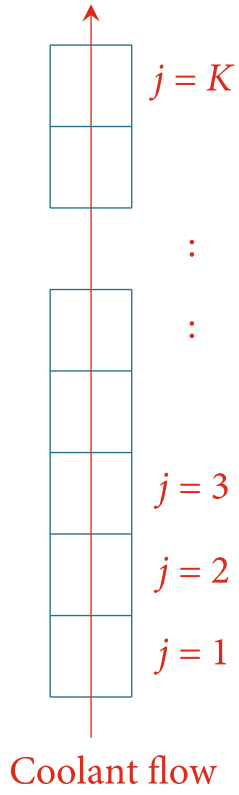

Figure 7: Axial discretization of the hottest fuel channel.

region. From this, the fuel outer surface temperature is calculated using the cladding inner surface temperature as

$$T_{j,f}(r_f) = T_{j,\mathrm{ic}} + \frac{q'_j}{2\pi h_g} \ln\left(\frac{r_{\mathrm{ic}}}{r_f}\right), \tag{15}$$

where h_g is gap conductance. Finally, to obtain the fuel centerline temperature, a one-dimensional conduction model is solved in the fuel region. The centerline temperature can be calculated using the fuel surface temperature as

$$T_{j,f}(0) = T_{j,f}(r_f) + \frac{q'_j}{4\pi k_f}, \tag{16}$$

where k_f is the fuel conductance and r_f is the fuel pellet radius.

It should be noted that the hottest pin model is an approximate model. It is only used to set a lower limit for pin design reliability. For this reason, parameters like the material conductivity can be set to a conservative value with no need for a detailed model.

The initial thermal-hydraulic screening is used to eliminate designs with obviously high fuel and cladding temperatures. The user can control how many designs pass this screening process by adjusting the radial and axial peaking factors.

4.3. Multiphysics Analysis. The multiphysics analysis in this work was performed using the LMFR Utility for Physics Informed Nuclear Engineering (LUPINE) multiphysics simulation code [14, 28]. This code solves coupled neutronics, thermal hydraulics, and thermal expansion models and can perform depletion calculations, which enables fuel cycle analysis. The neutronics solver is based on the finite elements method (FEM). It employs a general unstructured mesh to solve the simplified P_N multigroup (SP_N) neutron transport equations with arbitrary truncation error N. The thermal-hydraulic model calculates the coolant temperature in each assembly at each axial level. Then, using a conduction model, the radial material temperatures in the fuel pin are calculated. Based on the average material temperatures, the thermal expansion model expands the finite volumes while preserving the material masses. The coupled multiphysics equations are solved simultaneously using a Picard iteration. Following the neutronic solution, the thermal hydraulics and thermal expansion solutions are calculated. Using the component temperatures and the expanded material number densities, the cross sections are updated in preparation for the next iteration. The single physics solvers are part of the code, and all operations are performed internally within LUPINE.

The depletion model of LUPINE depletes each individual assembly at each axial level. It uses a Chebyshev rational approximation method (CRAM) solver to solve the depletion matrix [29]. With these capabilities, LUPINE can accurately calculate nuclide number densities in the core through the fuel cycle. LUPINE also enables the easy handling of reactivity coefficient calculation.

Mesh regions in LUPINE are modeled as smeared material regions. This is a standard practice in LMFR modeling, given the large fast neutrons mean-free path. Cross sections for LUPINE are generated by the MC^2-3 code [30] developed by Argonne National Laboratory. The energy group structure used in all simulations is the default 33-group structure in MC^2-3. To support the multiphysics calculations, microscopic cross sections are generated at four different temperatures, and LUPINE interpolates the cross sections using local temperatures. The fuel temperature is interpolated with a square-root interpolation.

For the accurate modeling of LMFRs, the straightforward approach is to generate a unique cross-section library for each of the designs being modeled. However, such a practice would impose a large computational burden on the design process. Instead, a single microscopic cross-section library was generated for the reference design, and this library was used for all designs. Since it is a microscopic cross-section library, the density and geometric variations are accounted for by adjusting the number of densities. All the microscopic cross sections are still a function of temperature. To evaluate the effect of using a single microscopic cross-section library in the design process, the final optimized core was rerun using the reference cross-section library and a library generated specifically for the optimized core. The difference between the two results was less than 30 (pcm), which shows that using a single microscopic cross-section library is accurate.

In the current implementation of DOM, the multiphysics methodology only considers neutronics, thermal hydraulics, and thermal expansion. As a future development, the methodology can be enhanced by introducing fuel performance and shutdown margin in the decision-making process. Additionally, a full safety analysis on the designs found by DOM is necessary to assure the safe operation of the core.

4.4. Post Processing. This subsection describes the last three steps in the process of designing LMFRs using DOM (Figure 4).

Once the multiphysics analysis is done for all design samples that survived the initial thermal-hydraulic screening, the results are analyzed. The design parameters are determined and compared to the design constraints. If the design violates the design constraints, it will be excluded from further processing. If the design shows compliance with the constraints, an objective function is determined. In this work, the objective of the search process was to minimize the LFCC. Based on this, LFCC was used as the cost function.

The LFCC is a quantity that measures the cost of the nuclear fuel cycle. It includes the cost of extraction of the ore, conversion, enrichment, fabrication, disposal, and carrying costs. It is worth mentioning that LFCC does not include capital or operation and maintenance (O&M) costs. In the LFCC analysis of this work, the fuel cycle component costs used are presented in Table 4. Additional assumptions used in performing the analysis are presented in Table 5. For more details on calculating the LFCC, the reader is referred to Al-Dawood [31].

Table 4: Fuel cycle component costs [1].

Cost type	Unit	Value
Ore cost	\$/lb	40
Conversion cost	\$/kg	10
SWU cost	\$/kg	70
Fabrication cost	\$/kgU	500
Decontamination and dismantling (D&D) rate	\$/month	82494
Disposal	$\$/MW_e.Hr$	1

Table 5: Additional fuel cycle cost component assumptions.

Item	Unit	Value
Escalation rate	%	0
Fabrication escalation rate	%	5
Preoperation carrying charges	%	6
Carrying charges rate	%	2
Property tax rate	%	0
Conversion loss	%	0.5
Fabrication loss	%	0.1
Enrichment loss	%	0.5
Feed enrichment	%	0.71
Tail enrichment	%	0.25
Conversion to enrichment time	Days	60
Enrichment to fabrication	Days	60
Fabrication to startup	Days	120
Capacity factor	%	93.5

Once the objective function is calculated for successful design samples, a seeding process is performed. A seed is defined as a design sample which is believed to be close to an optimum (local or global).

The process adopted in this work for seeding the search space is as follows. All design samples with the same number of pins per assembly are grouped together. The LFCC for all design samples in each group is calculated. The design sample that has the smallest LFCC in each group is selected as a seed. The seed can then be used as an initial guess to start the local optimization. The local optimization step is an optional step that was added to the original work of DOM described by Al-Dawood [31].

The search algorithm used in the local optimization is the Nelder-Mead algorithm [22]. The local optimization uses the same decision variables, thermal-hydraulic screening, and multiphysics evaluations as the seed designs. The local optimization is considered an optional step in DOM because there is an inherent trade-off between the number of seed evaluations and the effectiveness of the local search. If the number of seeds is reduced, the local search increases the overall effectiveness of the search. As the number of seeds increases, the local search is less effective in helping the search. Therefore, if the number of seeds is significant, the local search is not needed.

Table 6: Domain of the search space.

Explanatory variable	Range
Assembly pitch (cm)	[16.1, 16.3]
Pitch-to-diameter ratio	[1.1, 1.3]
Pin radius (cm)	[0.6, 0.9]
Active fuel height (cm)	[200, 350]
Inner core enrichment (%)	[7.21, 11]
Middle core enrichment (%)	[11, 12]
Outer core enrichment (%)	[12, 15]

5. Optimization of WLFR

DOM is suggested as a methodology for designing and optimizing LMFRs. In this section, the utilization of DOM is demonstrated. DOM was used to further optimize the WLFR design. The objective of the optimization was to reduce the LFCC while complying with the design constraints. The multiphysics analysis was performed using LUPINE. The fuel cycle analysis performed in this work uses the 2019 nuclear power capacity factor, which is 93.5%.

The domain of the search space is shown in Table 6. Since the WLFR is an existing design, it can serve as a good initial guess for the optimization. In addition, the design search space can be relatively tight because a good initial guess existed.

In the modeling and simulation for the design samples of this demonstration study, the EOC is considered to be reached once the core multiplication factor drops below the critical eigenvalue, which is considered to be 1.004373. This value was selected to match the 25 EFPY cycle length calculated for the original design [1].

From the search space, 1500 samples were generated using LHS. Of these, 34.5% (518 samples) passed the initial thermal-hydraulic screening. For each of these, LUPINE was used to perform the multiphysics simulation. Each design sample was depleted until the EOC. The simulation results for each case were then compared to the design constraints. From the cases that pass the second screening, one seed design sample is presented along with the original design from Westinghouse in Table 7.

An LFCC analysis was performed for the original WLFR design. It was found that LFCC for this design was \$6.98/MW_e.hr. This value is smaller than the LFCC reported for the original design [1]. The differences are expected to be due to different methodologies and costs in accounting for LFCC. The detailed economic model used for the original WLFR is not known. For example, the values used in Table 5 were not reported for the original WLFR design [1]. However, it should be noted that the LFCC cost used for all the designs presented in this paper is consistent which qualifies a qualitative comparison between the designs.

The seed design can maintain criticality for 27.6 EFPY compared to 25 EFPY for the original design. The seed design achieves a 2.8% reduction in the LFCC, with a value of \$6.79/MW_e.hr. This reduction corresponds to about \$18 million of savings over the life of the reactor. The maximum and average burnup in the seed design is 190 MWd/kgHM and 119 MWd/kgHM, respectively.

Table 7: Comparison of original, seed, and optimized WLFR.

Parameter	Original design	Seed design	Optimized design
Assembly pitch (cm)	16.3	16.25	16.158
Pitch-to-diameter ratio	1.143	1.1296	1.1219
Number of fuel pins per assembly	61	61	61
Fuel pellet radius (cm)	0.7524	0.7594	0.7613
Fuel pin radius (cm)	0.8485	0.8564	0.8584
Fuel pin pitch (cm)	1.8925	1.8889	1.8795
Active fuel height (cm)	220	220	215.7
Inner core enrichment (%)	10.300	10.084	10.088
Middle core enrichment (%)	11.800	11.264	11.322
Outer core enrichment (%)	13.800	14.552	14.898
Cycle length (EFPYs)	25	27.6	30.28
LFCC (MW_e.Hr)	6.98	6.79	6.69
BOC ^{235}U masses (kg)			
IC	2232	2227	2195
MC	2331	2267	2245
OC	5224	5612	5662
Core total	9787	10105	10102
BOC ^{238}U masses (kg)			
IC	19441	19854	19563
MC	17422	17857	17585
OC	32634	32956	32344
Core total	69496	70667	69493
BOC total core HM masses (kg)			
IC	21673	22080	21758
MC	19752	20123	19830
OC	37858	38569	38006
Core total	79284	80772	79595

The Nelder-Mead algorithm [22] is then used to perform local optimization for the seed design. The seed design is used as an initial guess for the Nelder-Mead algorithm. The optimized design is also presented in Table 7. The optimized design has an LFCC of \$6.69/MW_e.hr, which is 4.2% lower than that of the original design, and it maintains criticality for 28.3 EFPY. This corresponds to a refueling interval of 30.28 years which is slightly longer than the 30 years requirement considering the capacity factor used in this paper. The average and maximum burnups in the optimized design are 123 MWd/kgHM and 195 MWd/kgHM, respectively. The multiplication factor profile as a function of depletion time for the original, seed, and optimized designs is presented in Figure 8. These results demonstrate the DOM capability to minimize the LFCC.

It should be noted that the improvement on the LFCC introduced to the WLFR using DOM is relatively small because the WLFR was already an optimized design. The strength of DOM is in the design of new cores, where no

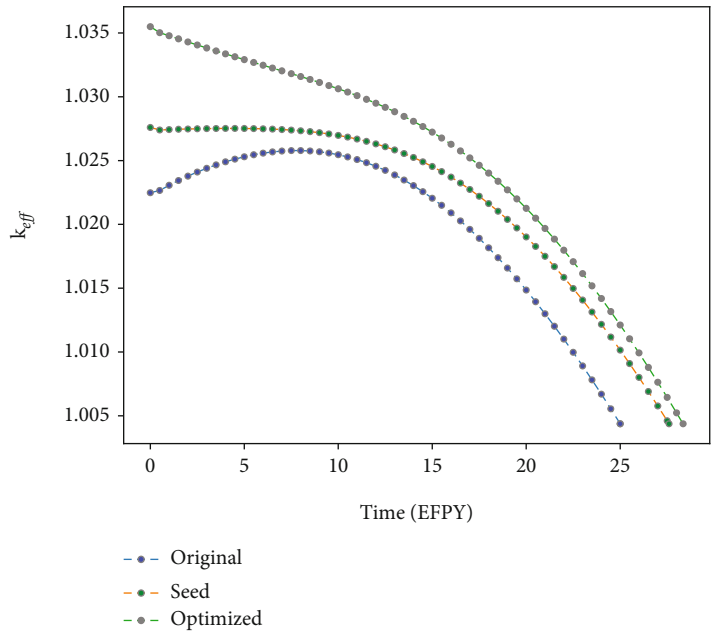

Figure 8: Multiplication factor as a function of depletion time for the optimized core.

Table 8: Isotope separation technologies pricing for ^{15}N enrichment according to Westinghouse estimates [32].

Technology	Cost $/g
Laser isotope separation	0.5-1
Chemical exchange	1.5-2
Ion exchange	1.6

"good" starting guess is available. This will be demonstrated in the next section.

6. ^{15}N Enrichment Investigation

Uranium nitride fuel is a candidate fuel for fast reactors, generally, and LFRs, specifically. This fuel offers several advantages over other types of fast reactor fuels. In comparison with oxide fuel, nitride fuel attains a larger fissile density which enables nitride fuel to achieve higher burnup. In addition, nitride fuel has a higher thermal conductivity and better compatibility with LMFR coolants. Compared to metallic fuel, nitride fuel has a higher melting point. Based on this, the nitride fuel has a potential to offer increased safety and economic performance.

Despite the advantages that UN offers, there are several challenges facing the utilization of this fuel. One of these is the relatively high neutron absorption cross section of ^{14}N which deteriorates the neutron economy of the core [1]. Additionally, the (n, p) reaction of ^{14}N results in the production of ^{14}C, which is a radiotoxic isotope that is characterized by a long half-life (5730 years) and high mobility in the environment. These issues can be alleviated by enriching the UN composition to >90% in ^{15}N. However, the problem of this approach is the lack of experience with ^{15}N enrichment technology on an industrial scale. Thus, there is a large uncertainty in the reported values of the cost of this enrichment process. Westinghouse reports that the estimated cost of ^{15}N enrichment using centrifuge process is about $35/g [32], which is considered a very high price. The report also suggests three isotopic separation technologies as an alternative for the centrifugal process. These technologies are summarized in Table 8 along with their estimated costs. In a more recent reference by Wallenius [33], it was highlighted that the currently used technology for ^{15}N enrichment is the isotopic exchange method. Wallenius mentioned that on a laboratory scale of a few kilograms per year, the cost of enrichment is $100/g of ^{15}N. The source also mentions that in order to make the ^{15}N enrichment process economically effective for fast reactor technology, the cost should be less than $10/g. Since the cost of enriched nitrogen is unknown, this work will search for a breakeven cost which will make the cost of an enriched nitrogen core equivalent to that of the original WLFR core.

An advantage of using ^{15}N compared to ^{14}N in the fuel is that ^{15}N has a lower absorption cross section compared to ^{14}N. The lower cross section can result in a reduced size core or reduced ^{235}U enrichment of the fuel, which presents an economic advantage. For these reasons, we attempted to explore the design of a ^{15}N-enriched UN-fueled long-life core LFR.

In this work, a second study is performed to demonstrate DOM. The objective was to design an economic long-life core LFR fueled with ^{15}N-enriched UN fuel. The core is referred to as the enriched nitrogen LFR (ENLFR). The core configuration used in this study is different from that of the WLFR. A midplane view of the new configuration for the ^{15}N-enriched core is presented in Figure 9. The domain of the search space utilized in the search for the ENLFR is presented in Table 9. This search space is wider than the one used to optimize the WLFR. This is because DOM is used

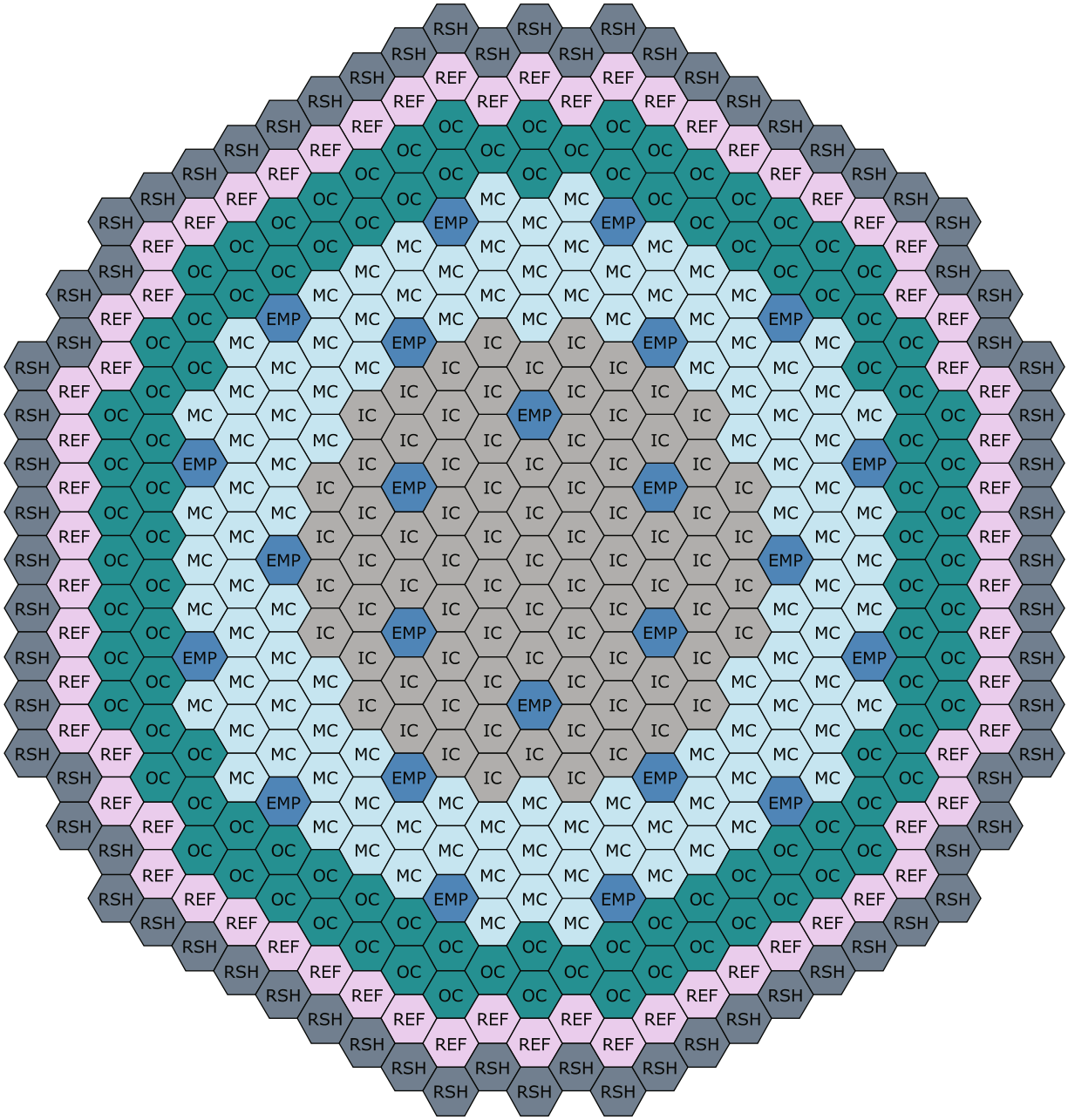

Figure 9: ^{15}N-enriched core configuration.

Table 9: Domain of the search space for the ENLFR.

Explanatory variable	Range
Pin radius (cm)	[0.4, 0.9]
Pitch-to-diameter ratio	[1.05, 1.3]
Assembly pitch (cm)	[14, 16.5]
Fuel height (cm)	[190, 250]
Inner core enrichment (%)	[9, 11]
Middle core enrichment (%)	[11, 13]
Outer core enrichment (%)	[12, 15]

here to perform a search without having a good initial guess, which helps in demonstrating the exploratory capability of DOM. The ^{15}N enrichment was considered to be 93%. The seed suggested by DOM is also presented in Table 10. No local optimization was performed in this study.

The multiplication factor profile as a function of depletion time in the ENLFR core is shown in Figure 10. The reactor can maintain criticality for 20.5 EFPYs, but the maximum burnup in the fuel will slightly exceed the constraint of 200 MW/kgHM. A cycle length of 20.3 EFPY will meet the maximum burnup constraint. The LFCC for this core design break-even with the original design LFCC of \$6.98/MW$_e$.hr occurs at a cost of ^{15}N enrichment of about \$14/g. This cost is at least 40% higher than the reported

Table 10: Seed design for the ENLFR.

Parameter	Seed design
Assembly pitch (cm)	16.106
Pitch-to-diameter ratio	1.1781
Number of fuel pins per assembly	91
Fuel pellet radius (cm)	0.5465
Fuel pin radius (cm)	0.6178
Fuel pin pitch (cm)	1.5244
Active fuel height (cm)	205.84
Inner core enrichment (%)	9.5345
Middle core enrichment (%)	12.791
Outer core enrichment (%)	14.259
Cycle length (EFPYs)	20.3
^{15}N enrichment (%)	93.0

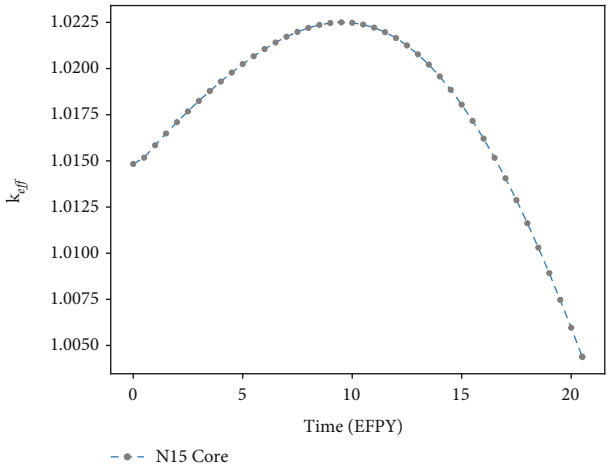

Figure 10: Multiplication factor as a function of time for the ^{15}N core.

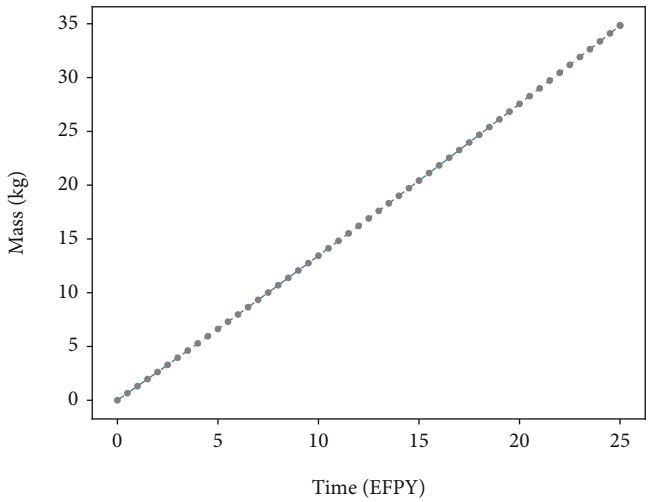

Figure 11: ^{14}C mass development as a function of time in WLFR.

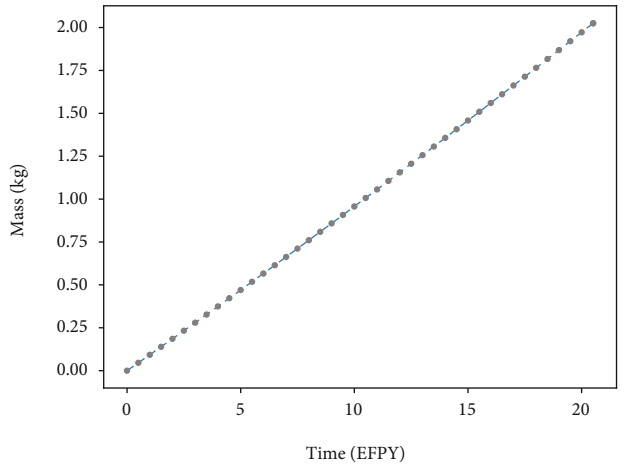

Figure 12: ^{14}C buildup in the ENLFR core.

value in Wallenius [33] for a fast reactor, which means the ENLFR is competitive at a higher enriched nitrogen cost. The ENLFR core lasts for a shorter cycle length compared to the natural nitride-fueled core (i.e., the WLFR). However, the goal of this design process is to find a core with a competitive fuel cycle cost. In addition, the cycle length of the ENLFR core is consistent with the cycle length constraint of the WLFR (as presented in Table 2) [1].

Another advantage of using ^{15}N-enriched UN fuel is a reduction of ^{14}C buildup in the core. Based on LUPINE simulation of the WLFR, the EOC ^{14}C mass developed is about 36 kg. Thus, the ^{14}C activity (α) at EOC is

$$\alpha = 160390 \text{ Ci}. \quad (17)$$

The buildup of the ^{14}C mass in the core as a function of depletion time is presented in Figure 11. Based on this, the specific activity due to ^{14}C in the fuel material is about 2000 Ci per metric ton initial heavy metal (MTHM). To facilitate a comparison, the specific activity of ^{14}C in LWR spent fuel is less than 2 Ci/MTHM [34]. Worth mentioning is that MC^2-3 does not include the ^{14}C isotope cross section in the library but has the natural carbon cross section. The carbon isotopes, ^{12}C and ^{14}C, have similar energy-dependent cross sections, which are small in the fast energy range. Based on this, a judgment was made to use the ^{12}C cross section in order to model the neutron absorption in ^{14}C through the simulation. The amount of ^{14}C in the core at EOC is about 2 kg, which corresponds to about 160 Ci/MTHM. The buildup of ^{14}C isotope mass as a function of time is presented in Figure 12.

7. Conclusions

This work presented the design and optimization methodology (DOM) for LMFRs. The method is based on the effective sampling of the search space and the identification of invalid designs through an initial screening before performing multiphysics analysis. DOM was demonstrated through two studies. The objective in both studies was to reduce the LFCC. A 4.2% reduction on LFCC was achieved compared to the original design. In the second study, DOM was used to design a long-life core ^{15}N-enriched UN-fueled core (referred to as the ENLFR) with an economically

competitive fuel cycle. It was found that a competitive LFCC for the ENLFR can be achieved if the ^{15}N enrichment cost is \$14/g or lower.

The paper also calculated the buildup of the ^{14}C in both the WLFR and the ENLFR core. It was found that the ^{15}N enrichment process can significantly reduce the buildup of ^{14}C in the core.

Data Availability

The core design data used to support the findings of this study are available from the corresponding author upon request.

Conflicts of Interest

The authors declare that they have no conflicts of interest.

References

[1] T. Kim, N. Stauff, C. Stansbury, A. Levinsky, and F. Franceschini, "Long Core life design options for the Westinghouse LFR," in *Proceedings of International Nuclear Fuel Cycle Conference (GLOBAL)*, Seattle, WA, USA, 2019.

[2] G. Grasso, C. Petrovich, D. Mattioli et al., "The core design of ALFRED, a demonstrator for the European lead-cooled reactors," *Nuclear Engineering and Design*, vol. 278, pp. 287–301, 2014.

[3] I. S. Hwang, S. Jeong, B. Park, W. Yang, K. Suh, and C. Kim, "The concept of proliferation-resistant, environment-friendly, accident- tolerant, continual and economical reactor (PEACER)," *Progress in Nuclear Energy*, vol. 37, no. 1-4, pp. 217–222, 2000.

[4] D. J. Kropaczek and P. J. Turinsky, "In-core nuclear fuel management optimization for pressurized water reactors utilizing simulated annealing," *Nuclear Technology*, vol. 95, no. 1, pp. 9–32, 1991.

[5] D. J. Kropaczek, "COPERNICUS: a multi-cycle optimization code for nuclear fuel based on parallel simulated annealing with mixing of states," *Progress in Nuclear Energy*, vol. 53, no. 6, pp. 554–561, 2011.

[6] M. I. Radaideh, I. Wolverton, J. Joseph et al., "Physics-informed reinforcement learning optimization of nuclear assembly design," *Nuclear Engineering and Design*, vol. 372, article 110966, 2021.

[7] J. Fran, "A practical optimization procedure for radial BWR fuel lattice design using tabu search with a multiobjective function," *Annals of Nuclear Energy*, vol. 30, no. 12, pp. 1213–1229, 2003.

[8] D. Babazadeh, M. Boroushaki, and C. Lucas, "Optimization of fuel core loading pattern design in a VVER nuclear power reactors using particle swarm optimization (PSO)," *Annals of Nuclear Energy*, vol. 36, no. 7, pp. 923–930, 2009.

[9] M. D. DeChaine and M. A. Feltus, "Nuclear fuel management optimization using genetic algorithms," *Nuclear Technology*, vol. 111, no. 1, pp. 109–114, 1995.

[10] S. Qvist and E. Greenspan, "The ADOPT code for automated fast reactor core design," *Annals of Nuclear Energy*, vol. 71, pp. 23–36, 2014.

[11] X. Luo, X. Zhang, S. Wang, R. Jiang, and H. Chen, "Automated core design code development for a lead-cooled fast reactor and its core optimization," *International Journal of Energy Research*, vol. 45, no. 8, pp. 11721–11734, 2021.

[12] H. Chen, X. Zhang, Y. Zhao et al., "Preliminary design of a medium-power modular lead-cooled fast reactor with the application of optimization methods," *International Journal of Energy Research*, vol. 42, no. 11, pp. 3643–3657, 2018.

[13] W. Barthold, "CONSTRAINED NUCLEAR DESIGN," in *Advanced Reactors: Physics Design and Economics*, J. Kallfelz and R. Karam, Eds., pp. 731–739, Elsevier, Atlanta, Georgia, 1975.

[14] W. C. Dawn and S. Palmtag, "A Multiphysics simulation suite for liquid metal-cooled fast reactors," *Annals of Nuclear Energy*, vol. 159, article 108213, 2021.

[15] T. D. C. Nguyen, M. F. Khandaq, E. Jeong, J. Choe, D. Lee, and D. A. Fynan, "MicroURANUS: core design for long-cycle lead-bismuth-cooled fast reactor for marine applications," *International Journal of Energy Research*, vol. 45, no. 8, pp. 12426–12448, 2021.

[16] J. Park, T. Tak, T. Kim et al., "Design study of long-life small modular sodium-cooled fast reactor," *International Journal of Energy Research*, vol. 41, no. 1, pp. 139–148, 2017.

[17] C. Wang, S. Wei, W. Tian, S. Qiu, and G. Su, "RETRACTED: core design and analysis of a lead-bismuth cooled small modular reactor," *Annals of Nuclear Energy*, vol. 133, pp. 511–518, 2019.

[18] H. Sekimoto, K. Ryu, and Y. Yoshimura, "CANDLE: the new burnup strategy," *Nuclear Science and Engineering*, vol. 139, no. 3, pp. 306–317, 2001.

[19] J. J. Sienicki, A. Moisseytsev, W. S. Yang et al., "Status Report on the Small Secure Transportable Autonomous Reactor (SSTAR)/Lead-cooled Fast Reactor (LFR) and Supporting Research and Development," Technical Report ANL-GenIV-089, Argonne National Laboratory, Argonne, IL, USA, 2008.

[20] K. Tucek, J. Carlsson, and H. Wider, "Comparison of sodium and lead-cooled fast reactors regarding reactor physics aspects, severe safety and economical issues," *Nuclear Engineering and Design*, vol. 236, no. 14-16, pp. 1589–1598, 2006.

[21] B. Adams, W. Bohnhoff, K. Dalbey et al., "DAKOTA a Multilevel Parallel Object-Oriented Framework for Design Optimization, Parameter Estimation, Uncertainty Quantification, and Sensitivity Analysis: Version 6.14 User's Manual," Technical Report SAND2021-5822, Sandia National Laboratory, Albuquerque, NM, USA, 2021.

[22] T. Santner, B. Williams, and W. Notz, *The Design and Analysis of Computer Experiments*, Springer, 2003.

[23] M. D. Mckay, R. J. Beckman, and W. J. Conover, "A comparison of three methods for selecting values of input variables in the analysis of output from a computer code," *Technometrics*, vol. 42, no. 1, pp. 55–61, 2000.

[24] J. L. Deutsch and C. V. Deutsch, "Latin hypercube sampling with multidimensional uniformity," *Journal of Statistical Planning and Inference*, vol. 142, no. 3, pp. 763–772, 2012.

[25] S. Moza, "sahilm89/lhsmdu: Latin Hypercube Sampling with Multi-Dimensional Uniformity (LHSMDU): Speed Boost minor compatibility fixes," *Zenodo*, vol. 10, 2020.

[26] W. Pfrang and D. Struwe, "Assessment of Correlations for Heat Transfer to the Coolant for Heavy Liquid Metal Cooled Core Designs," Technical Report FZKA-7352, Forschungszentrum Karlsruhe GmbH, Karlsruhe, 2007.

[27] C. Fazio, V. P. Sobolev, A. Aerts et al., "Handbook on Lead-Bismuth Eutectic Alloy and Lead Properties, Materials Compatibility, Thermal-Hydraulics and Technologies-2015 Edition," Technical Report NEA-7268, Organisation for Economic Co-Operation and Development, 2015.

[28] K. Al-Dawood, W. C. Dawn, and S. Palmtag, "Multiphysics simulation of uranium-nitride fueled lead-cooled fast reactor," in *ANS M&C 2021 – The International Conference on Mathematics and Computational Methods Applied to Nuclear Science and Engineering ANS*, Raleigh, NC, USA, 2021.

[29] S. Palmtag, W. Dawn, and C. Lawing, "Fast reactor depletion methods in LUPINE," in *ANS M&C 2021 – The International Conference on Mathematics and Computational Methods Applied to Nuclear Science and Engineering ANS*, Raleigh, NC, USA, 2021.

[30] C. H. Lee and W. S. Yang, *MC2-3: Multigroup Cross Section Generation Code for Fast Reactor Analysis*, Technical Report ANL/NE-11-41 Rev. 2, Argonne National Laboratory, Argonne, IL, USA, 2013.

[31] K. A. Al-Dawood, "Modeling, Simulation and Optimization of Lead-Cooled Fast Reactors, [M.S thesis]," North Carolina State University, Raleigh, NC, 2021.

[32] E. J. Lahoda and F. A. Boylan, "Development of LWR Fuels with Enhanced Accident Tolerence," Technical Report RT-TR-15-34, Westinghouse Electric Company, 2015.

[33] J. Wallenius, "Nitride Fuels," in *Comprehensive Nuclear Materials*, R. J. Konings and R. E. Stoller, Eds., pp. 88–101, Elsevier, Oxford, 2nd edition, 2020.

[34] R. Van Konynenburg, "Behavior of carbon-14 in waste packages for spent fuel in a tuff repository," *Waste Management*, vol. 14, no. 5, pp. 363–383, 1994.